Chapter 12

Evaluation of Solidification Times for Medium and High Carbon Steels Based upon Heat Transfer and Solidification Phenomena in the Continuous Casting of Blooms

Panagiotis Sismanis

Additional information is available at the end of the chapter

http://dx.doi.org/10.5772/60706

1. Introduction

The quest for billets and blooms production in the continuous casting of carbon steels with more stringent quality demands in internal soundness, free from surface defects, and internal porosity has increased the need for more insight in the appraisal of the phenomena associated with solidification under industrial conditions. Medium and high carbon steels cover a broad range of manufacturing products; nevertheless, the production of this type of material with a constant high percentage of prime-choice products remains a tough subject to analyze, understand, and more difficult to attain in practice. These carbon steels exhibit relatively low liquidus and solidus temperatures, with these values decreasing even further as carbon levels increase. It is understood that the blooms produced must be 100% crystallized (solid) at least before cutting to the delivered lengths is accomplished. It is realized that the larger the cross-section of the produced cast product the more time it requires in order to solidify completely. Big-sized cast products (or blooms) are more desirable for mainly two reasons: (a) large cross-sections are associated with large values of mass per unit length, hence, productivity is favored, and more important (b) large cross-sections are subject to larger values of area reduction once rolled, giving products with smaller possibility to quality degradation. On the other hand, the proper control of the cooling intensity in the secondary cooling zones (air-mist spray zones) upon the solidifying product in order to avoid surface/sub-surface defects in the unbending regions of the caster, places limitations on the casting speeds, and therefore productivities are not always at the desired levels. In practice, fundamental operation parameters like casting speed, casting temperature, and cooling-water consumption at the secondary (spray) zones

per produced mass of steel are among the most critical ones that the operator should keep in mind, once these have been analyzed, and their impact upon quality has been realized. Furthermore, from the early stages of medium and high-carbon steels casting, the operator has appreciated that it has been impossible to attain the high levels of productivity as with low and medium-low carbon steels without loss of internal quality. This is so because the low solidus temperatures that these grades exhibit become even lower in a dynamic way due to the local cooling rates that affect the solidification mechanism. Indeed, micro-segregation phenomena become more pronounced for these types of steels reducing even further the temperature at which the product becomes 100% solid, or in other terms, the solid fraction becomes one. There are some correlations for the solidus temperatures that unfortunately do not hold appreciably well, under varying cooling conditions, as it normally happens in the industrial continuous casting process. Nevertheless, the liquidus temperature is computed with great precision based upon the liquid-steel chemical analysis, and in this way, the industrial parameter known as superheat, which is the difference between the casting and liquidus temperatures, is calculated correctly; it is known that superheat is of paramount importance in the casting process. In this study, an attempt was carried out in order to shed some light into the effect of the various casting parameters upon the internal quality of the produced blooms in the continuous caster of Stomana, Pernik, Bulgaria. The biggest size of blooms produced currently in this caster is 300 x 250 mm x mm, and most medium and high-carbon grades are produced in this size. A heat transfer and a micro-segregation model were coupled and put into effect in order to facilitate the analysis of solidification along the caster length. Consequently, the solid fraction in the mushy zone, which is actually the intermediate zone between liquid and solid, was computed across a bloom section at any point along the caster, or in other words, from the meniscus level in the mold till the point of analysis. In addition to this, temperature and local-cooling rate distributions were also computed in a similar manner. Different operating conditions were fed into the simulation model in order to compute the required metallurgical lengths, or in other words, the effective cutting lengths that obeyed the unity solid fractions in the mushy zone along the centerline of a bloom.

2. Quality problems associated with internal soundness/central porosity

From the early times of the continuous casting for medium and high carbon steels, it has been realized that central porosity as a quality problem seems inevitable. Figure 1 shows a picture from a macro-etched high carbon bloom cross-section.

It is pointed out that for high carbon steels the tendency for central porosity generation is very large no matter how well liquid steel is treated, and how successful the casting process is performed. With time, the continuous casters manufacturers realized that this problem can be abided if electromagnetic stirring (EMS) was applied not only in the mold but in specific positions along the strand, mostly known as strand (S-EMS) and final (F-EMS) positions. F-EMS position is considered the position at which the mushy zone along the centerline becomes solid, or the position around the final solidification of the product. This is an effective technical solution to lessen the problem and is currently applied in some caster installations worldwide.

http://dx.doi.org/10.5772/60706

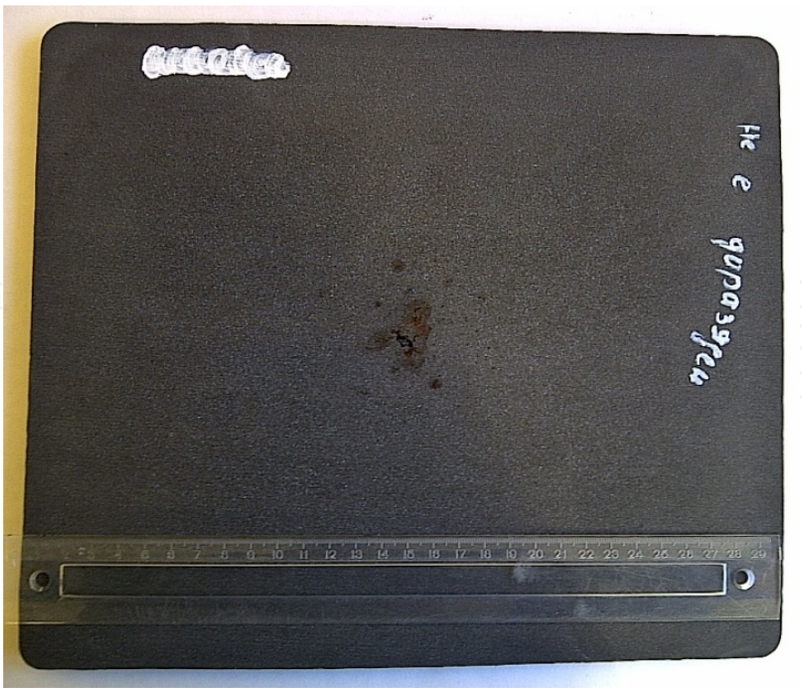

Figure 1. A macro etched cross-section from a 300 x 250 mm x mm bloom. The central porosity, which creates an internal-soundness quality problem, is apparent for this high-carbon cast product.

Another promising technical solution is the dynamic soft reduction, in which the part of the bloom which approaches final solidification is subject to a compressive force that slightly reduces its size in one direction but mechanically eliminates the central porosity problem. It is interesting to note that there are installations worldwide that currently apply both technical solutions for internal porosity minimization. However, no matter whether an installation applies one technical solution or another, it is really intriguing to try to figure out why and how this happens, and most importantly up to what extent, depending upon the various casting operating conditions. Without some knowledge upon this problem for a specific installation, one may not appreciate all the phenomena involved in, and maybe a definitive solution may not be successfully attained even after the installation of the discussed technical solutions. That is why it was decided to get some extra information on the subject before the installation of any technical solution might be applied at the Stomana bloom caster.

3. Literature review mostly oriented to quality problems for medium and high carbon steels

Superheat was one of the most fundamental factors recognized from the early years of continuous casting especially for medium and high carbon steels. In an early report [1], pilot plant tests were performed casting 150 x 150 mm x mm billets of high carbon steels. It was proven that at low superheats or even sub-liquidus casting temperatures, the centerline segregation was minimized. The electromagnetic stirring at the mold (M-EMS) exhibited some benefits, and the application of EMS at the strand (S) and final (F) stages of solidification started

being installed in some casters worldwide. In a study [2], it was found that the combination of EMS, that is, (S+F)-EMS for blooms and (M+S+F)-EMS for billets, is the most effective method for reducing macro-segregation among various EMS conditions, causing them to solidify more rapidly during the final stages of solidification, providing more finely distributed porosities and segregation spots along the central region. The optimum liquid pool thickness was found to decrease as the carbon content increased, which may be attributed to longer solidification times in the solid fraction range from f_s= 0.3 to 0.7. By gaining experience [3] in an actual caster installation, they concluded that a mold tube with a parabolic taper was proven good enough quality-wise for the continuous casting of medium and high carbon steels for carbon contents up to 0.55%. In another study [4], a coupled model was developed consisting of a cellular automaton scheme (CA) simulating the grain structure formation during solidification, and a finite difference scheme simulating the macroscopic heat transfer and solute transport in the continuous casting process. Columnar to equiaxed dendritic transition was effectively reproduced. The effect of superheat on the solidification structure was analyzed, verifying the empirical fact that increasing superheat the columnar dendritic growth increases against the equiaxed one. Under industrial conditions [5], S-EMS applied in the continuous casting of 150 x 150 mm x mm billets reduced centerline segregation up to a degree. However, increasing field intensity, deterioration upon the attained quality improvement was recorded. Some interesting fundamental research, as well as industrial achievements regarding medium and high carbon steels were presented in the recent European continuous casting conference [6-18], revealing the broad research and practice that may be developed in the field during the coming years. In Ref. [6], they used the liquid–solid interface energy as the main property in order to study the micro-segregation during solidification. They concluded that convection effects influenced micro-segregation behavior of the studied high carbon (C ≤ 0.7%), and high manganese steels. In another work [7], a 3D mathematical model was used to analyze the characteristics of magnetic field, flow field, and solidification of molten steel in the mold with electromagnetic stirring for a 260 x 300 mm x mm bloom. A dominant swirling motion at the transverse direction described the flow in the mold; the electromagnetic field was computed with similar values to those measured. They took under consideration the air-gap formation in the corners of the bloom adjacent to the mold. A summary of the actions taken to increase the productivity of Tenaris casters and to ensure high-quality standards in the produced round blooms for low, medium, and high carbon steels was presented in Ref. [8]. An in-house heat transfer model was developed to simulate the temperature distribution at various casting conditions. In addition to this, a rigid-viscoplastic model for simulating the thermal strain effects was developed to assess the potential risk of internal and surface cracks. Industrial practice was improved [9] in the field of high-carbon steel casting by the introduction of EMS not only in the mold, but in specific positions in the strand, and sometimes in the position of the final solidification front. Typical values for solid fraction along the central axis where the F-EMS is effective were found to be in the range of 0.1–0.4. Just for the sake of sense, comparing the findings between the published works [2] and [9] for the valid solid-fraction range for a successful F-EMS application, it is derived that depending upon a specific caster installation different approximations may yield to optimum solutions. In a recent monumental industrial installation [10], the excellent quality results in the production of –among others – medium and high carbon steels were successfully attained by a 2-strand vertical caster (in order to avoid extra strains from the bending/unbending of the strand, which are inevitable to customary

http://dx.doi.org/10.5772/60706

curved casters) for the production of big sections of blooms (up to 420 x 530 mm x mm). The caster managed to attain high quality results with the simultaneous application of a soft reduction system plus a moveable F-EMS system per strand. Chaotic phenomena seem to take place [11] in the continuous casting of steel billets, and specifically porosity chains seem to follow chaotic behavior along a cast billet. In other words, the chain of voids that are formed in the central zone along a billet and are generally coupled with segregation exhibit a spacing fluctuation in an erratic, random manner; stochastic modelling was applied on the basis of empirical time series in order to capture much of the dynamics. The lowering of the solidus temperature with respect to carbon-content increase for steels seems to be magnified by the boron effect [12]. Indeed, high Mn medium carbon steels with B higher than 40 ppm exhibit a very low solidification temperature at about 1140°C. In general, it has been verified that for high carbon steels (C≤1%), the addition of B introduces the possibility of a retrograde melting phenomenon retaining liquid at temperatures around 1100°C. In actual practice, a proper secondary cooling scheme should be applied in order to minimize re-melting behavior. In a similar study [13], low and medium carbon boron-steels (B≈30–40 ppm) exhibit a sharp decrease of hot ductility at about 1100°C for a 0.7%Mn content. It was explained on the basis of BN formation after the initial MnS formation; castability is therefore reduced for these types of steels. The implementation of soft reduction at the Voestalpine Stahl Donawitz bloom caster for the continuous casting of high carbon (0.80–1.05%C) rounds exhibited positive quality results [14]. On the other hand, the EMS underlined the proper positioning limitations that made the implementation very difficult to attain reliable and reproducible quality results. Proper design can be successful in as far as quality results are concerned even for small radius casters. In a revamping case [15], good quality results were obtained in a relatively small radius (~5m) caster through multi-radius unbending. Furthermore, the addition of M-EMS, S-EMS, and F-EMS gave rise to the successful casting of medium and high carbon steels with billets cross-sections of 110 x 110 up to 160 x 160 mm x mm. Proper design by reducing roll pitch in the areas where soft reduction was applied and implementing EMS and proper secondary cooling led to the required quality improvements in the revamping of another caster [16] for the production of high carbon steels. The need for fundamental research is illustrated in the following two published works. In the first one [17], an in situ material characterization by bending (IMC-B) 3-point-bending test was developed to simulate crack formation that takes place during continuous casting for most carbon grades; after the test, the strains were calculated using a simulation model in ABAQUS. In the next work [18], it was explicitly verified that micro-segregation phenomena are of paramount importance in the calculation of the final solidification front in order to apply soft reduction efficiently; specifically, an error of about 40°C in the estimation of the solidus temperature may result in an uncertainty of about 1.2 m in the determination of the correct soft reduction point.

4. Micro-segregation effects

The liquidus temperature for a specific steel chemical analysis is calculated with very good accuracy. However, the correct calculation of the solidus temperature is not always that easy. Nevertheless, there are some formulas for the computation of the solidus temperature based upon the specific chemical analysis. One is given by equation (1) as presented in reference [19]:

$$T_S^* = 1535 - 200(\%C) - 12.3(\%Si) - 6.8(\%Mn) - 124.5(\%P) - 183.9(\%S) - 4.3(\%Ni) - 1.4(\%Cr) - 4.1(\%Al) \quad (1)$$

The Simple model [20] for micro-segregation gives a thorough fundamental analysis for the computation of both the liquidus and solidus temperatures. According to this, the computation of the liquidus temperature is given by equation (2) based on chemical analysis only:

$$T_L = 1536 - 78(\%C) - 7.6(\%Si) - 4.9(\%Mn) - 34.4(\%P) - 38(\%S) - 4.69(\%Ni) - 1.04(\%Cr) - 5.32(\%Cu) - 2.6(\%Mo) - 10.24(\%Ti) - 12.95(\%V) - 10.24(\%Nb) - 0.24(\%W) - 60(\%N) \quad (2)$$

However, for the computation of the solidus temperature the same model [20] requires more computational effort, as the solid fraction in the mushy zone (in which solid and liquid co-exist) depends not only upon temperature but local cooling-rates as well. This can be described as:

$$f_S = G(T, C_R) \quad (3)$$

The function *G* includes the whole logic of calculation depending upon the phase of crystallization, that is, γ, δ, and/or peritectic. Most medium-high and high carbon steels crystallize in the γ phase. Table 1 shows the salient species for the two chemical analyses that were used in this study belonging in the category of medium-high (MC), and high carbon (HC) steels.

Type	T_L(°C)	T^*_S(°C)	T_S(°C)	C	Si	Mn	P	S	Cr	V
HC	1466	1366	1325	0.77	0.28	0.76	0.01	0.02	0.32	0.00
MC	1493	1435	1404	0.44	0.23	0.63	0.01	0.02	0.08	0.00

Table 1. Chemical analyses with computed values for the liquidus and solidus temperatures

Equation (2) was used for the calculation of the liquidus temperatures, and equation (1) for the solidus temperature T^*_S. Nevertheless, in order to have more uniform and comparable results, the solidus temperature T_S based on the simple model of micro-segregation analysis was computed at very low cooling rates (10^{-12} °C/sec) for both steel grades, respectively. Figures 2 and 3 illustrate the effect of micro-segregation upon the solidus temperature and show a form for function *G* at various levels of cooling rates. It is interesting to note that in both cases, the larger the cooling rate the lower the solidus temperature. On the other hand, the solidus temperatures that were computed by equation (1) are by far above the corresponding values computed by the micro-segregation analysis even at moderate local cooling rates. Furthermore, the biggest difference is computed at the lowest selected cooling rate (10^{-12} °C/s) for both cases; this extreme low value for the local cooling rate was adopted in order to simulate – as much as possible – the solidus temperature at infinite time of crystallization.

http://dx.doi.org/10.5772/60706

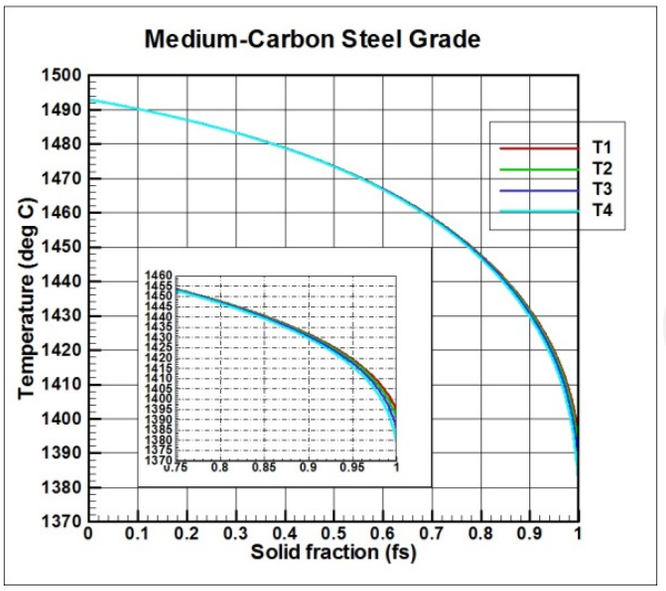

Figure 2. Micro-segregation results for the selected medium carbon steel at various levels of cooling rates: (T1) C_R= 0.01 °C/s, T_S = 1394°C; (T2) C_R= 0.10 °C/s, T_S = 1391°C; (T3) C_R= 1.0 °C/s, T_S = 1385°C; (T4) C_R= 10.0 °C/s, T_S = 1379°C.

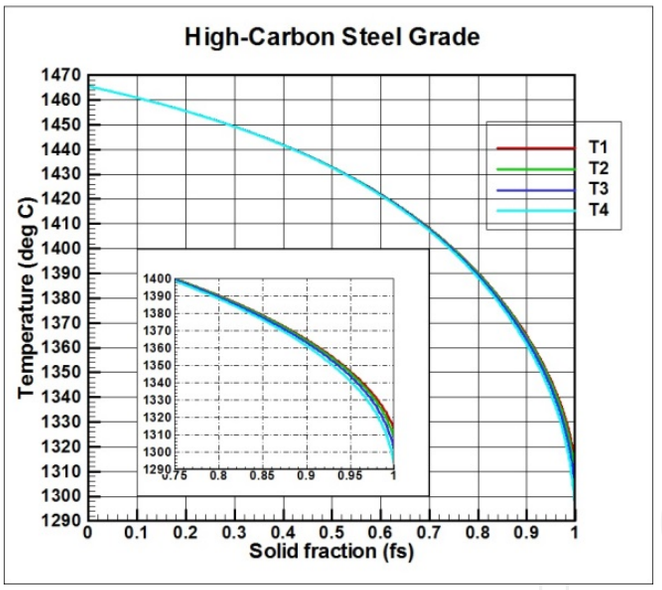

Figure 3. Micro-segregation results for the selected high carbon steel at various levels of cooling rates: (T1) C_R= 0.01 °C/s, T_S = 1313°C; (T2) C_R= 0.10 °C/s, T_S = 1308°C; (T3) C_R= 1.0 °C/s, T_S = 1301°C; (T4) C_R= 10.0 °C/s, T_S = 1292°C.

5. Heat-transfer mathematical approach

The general 3D heat-transfer equation that describes the temperature distribution inside the solidifying body is given by the following equation according to Refs. [21, 22]:

$$\rho C_P \frac{\partial T}{\partial t} = \nabla \cdot k \nabla T + S \tag{4}$$

The source term S may be considered [23] to be of the form:

$$S = S_C + S_P \cdot T \tag{5}$$

Furthermore, T is the temperature, and ρ, C_p, and k are the density, heat capacity, and thermal conductivity, respectively. The heat transfer equation in Cartesian coordinates may be written as:

$$\rho C_P \frac{\partial T}{\partial t} = \frac{\partial}{\partial x}\left(k \frac{\partial T}{\partial x}\right) + \frac{\partial}{\partial y}\left(k \frac{\partial T}{\partial y}\right) + S \tag{6}$$

The boundary conditions applied in order to solve (6) are as follows.

The heat flux in the mold was computed based on a recent treatment [7] that takes under consideration the air gap formation at the corners of the bloom, in conjunction with another older analysis [24] that came up with more precise heat-transfer coefficients in the mold. In the latter, the heat transfer coefficient at any position inside the mold is given by:

$$h_{m,z} = 1.35 \cdot 10^{-3}\left(1 - 0.8z\right) q_m \tag{7}$$

The heat flux at any position in the mold is given by:

$$q_z = a - b\sqrt{z}, \quad a = 2.680 \cdot 10^6, \quad b = 2.59578 \cdot 10^6, \quad 0 \le z \le L_m \tag{8}$$

Integrating (8), the average value for heat flux that is transferred through the walls of the mold is:

$$q_m = a - \left(\frac{2}{3} b\right)\sqrt{L_m} \tag{9}$$

Finally, the mold heat transfer coefficient was adjusted for the air-gap effect at the corners of the bloom [7], according to the following sets of equations:

$$h_{m,ag,z} = f_{corner} * h_{m,z}$$

$$f_{corner} = \begin{cases} 1.0 & 0 \le z \le 0.1L_m \\ 0.7 & 0.1L_m \le z \le 0.25L_m \text{ for the corner region(†), and 1.0 elsewhere} \\ 0.5 & 0.25L_m \le z \le L_m \text{ for the corner region(†), and 1.0 elsewhere} \\ (\dagger) & \text{Corner region: } (a_g W_x) \text{ along x-axis, } (a_g W_y) \text{ along the y-axis} \end{cases} \tag{10}$$

This formulation reasonably neglects the effect of contact resistance between the solidified shell of steel and the copper mold; this is a valid approach for blooms and big sections

http://dx.doi.org/10.5772/60706

generally, as the soft shell bulges a bit and stays in contact with the copper mold in the central areas of the mold, retracting somewhat at the corners. Furthermore, this analysis was performed on similar sized sections (300 x 260 mm x mm) [7]. The heat fluxes due to water spraying and strand radiation in the secondary cooling zones were calculated using the following expressions:

$$\begin{aligned} q_s &= h_s \cdot (T - T_{w0}) \\ q_r &= h_r \cdot (T - T_{env}) \quad \text{with } h_r = \sigma\varepsilon \cdot \frac{T^4 - T_{env}^4}{T - T_{env}} \\ q_c &= h_c \cdot (T - T_{env}) \end{aligned} \tag{11}$$

where h_s, h_r, and h_c are the heat transfer coefficients for spray cooling, radiation, and convection, respectively, T_{w0} is the water temperature, T_{env} is the ambient temperature, σ is the Stefan–Boltzmann constant, and ε is the steel emissivity (considered equal to 0.8 in the present study). Natural convection was assumed to be the prevailing convective mechanism, as stagnant airflow conditions were considered due to the low casting speeds of the strands applied in practice. The strand was assumed to be a long horizontal cylinder with an equivalent diameter of a circle having the same area with that of the cross-section of the bloom, and a correlation valid for a wide Rayleigh number range [25] was applied, written in an appropriate form [26]:

$$\sqrt{Nu_D} = 0.60 + 0.387 B^{1/6} \qquad B = Ra_D \left[1 + \left(\frac{0.559}{\mathrm{Pr}} \right)^{9/16} \right]^{16/9} \qquad \left(10^{-5} < B < 10^{13} \right) \tag{12}$$

where *Nu*, *Ra*, and *Pr* are the dimensionless Nusselt, Rayleigh, and Prandtl numbers, respectively. In this way, h_c is calculated by means of the Nu_D number. It is worth mentioning, however, that the radiation effects are more pronounced than the convection ones in the continuous casting of steels. From various expressions proposed in the literature for the heat transfer coefficient in water-spray cooling systems, the following formula was applied as approaching the present casting conditions:

$$h_S = 1570 \cdot W^{0.55} \cdot \frac{1 - 0.0075 T_{w0}}{4} \tag{13}$$

where *W* is the water flux for any secondary spray zone in liters/m^2/sec, and h_s is in W/m^2/K. At any point along the secondary zones (starting just below the mold) of the caster, the total heat flux q_{tot} is computed according to the following formula, taking into account that q_s may be zero at areas where no sprays are present:

$$q_{tot} = q_s + q_r + q_c \tag{14}$$

In mathematical terms, considering one quarter-section of the bloom assuming symmetry is valid, the aforementioned boundary conditions below mold can be written in compact form:

$$-k\frac{\partial T}{\partial x}=\begin{cases}h_{m,ag,z}(T-T_{WF}) & \text{at } x=W_x, 0\le y\le W_y, 0\le z\le L_m\\ q_{tot} & \text{at } x=W_x, 0\le y\le W_y, z>L_m\end{cases}$$
$$-k\frac{\partial T}{\partial y}=\begin{cases}h_{m,ag,z}(T-T_{WF}) & \text{at } y=W_y, 0\le x\le W_x, 0\le z\le L_m\\ q_{tot} & \text{at } y=W_y, 0\le x\le W_x, z>L_m\end{cases} \tag{15}$$

where z follows the casting direction starting from the meniscus level inside the mold; the mold has an effective length equal to L_m, and W_x and W_y are the half-width (as seen along the horizontal x-axis) and half-thickness (as seen along the vertical y-axis) of the bloom, respectively. Due to symmetry, the heat fluxes across the central planes are considered to be zero:

$$-k\frac{\partial T}{\partial x}=0 \quad \text{at } x=0, 0\le y\le W_y, z\ge 0$$
$$-k\frac{\partial T}{\partial y}=0 \quad \text{at } y=0, 0\le x\le W_x, z\ge 0 \tag{16}$$

Finally, the initial temperature of the pouring liquid steel is supposed to be the temperature of liquid steel in the tundish:

$$T=T_0 \quad \text{at } t=0 \ \left(\text{and } z=0\right),\ 0<x<W_x,\ 0<y<W_y \tag{17}$$

The thermo-physical properties of carbon steels were obtained from an older published work [27], in which the properties were given as functions of carbon content for the liquid, mushy, solid, and transformation-temperature domain values; this also gave rise to the advantage of eliminating the source factor (S= 0) by absorbing all transformation heats in the heat capacity values.

6. Numerical solution

This specific article is part of a series of published works with respect to the numerical solution of the heat transfer equation in 2D and 3D domains [28-30]. The strongly implicit method as practiced by Patankar [23] was applied. Although a grid of 200 x 200 nodal points was sufficient to stabilize results with a maximum error of 10^{-2}°C for each nodal point in the bloom quarter-section, a final grid of 400 x 400 nodal points was selected for the final computations. The selected time interval (Δt) was 0.25 sec, and the space intervals (Δx, Δy) were about 0.376 mm and 0.313 mm for the horizontal (x-axis) and vertical (y-axis) directions, respectively. Figure

http://dx.doi.org/10.5772/60706

4 depicts the domain (quarter-section) upon which the computations took place. This specific section was also cut in four sub-sections in order to exploit the 4-cores of a professional DELL laptop, Latitude E4310, with 8 GB RAM, operating under Windows 7 Professional. The Gauss–Seidel algorithm for the iterative solution of the matrix of equations was applied, as it was proven as a very suitable scheme for the solution of the temperature distribution putting into effect the OpenMP instruction set for parallel computation. Over-relaxation was applied for the fastest possible convergence; the over-relaxation parameter used was $\omega = 1.870$, which has exhibited good results for these kinds of studies [28-32]. This specific piece of software was developed in GNU C++, version 4.8.1, supplied by TDM-GCC, and accessed through the open source, cross-platform IDE, Code::Blocks, version 13.12. Due to a very large number of data (~2–3 GB) stored in disk per run, a time span of about 30 minutes was required in order to cover the phenomena taking place top-to-bottom in the bloom caster. In summary, the main points of the computations included the following:

- Calculation of the temperature distribution inside a bloom cross-section at a specific location at the caster.
- Calculation of the local cooling-rates distribution at the same cross-section and position.
- Calculation of the solid fraction in the mushy zone at the same cross-section and position.

The dynamic computation of the solidus temperature (at the solid fraction value equal to 1, $f_s = 1$) defined the border of the new solidification front of the mushy zone.

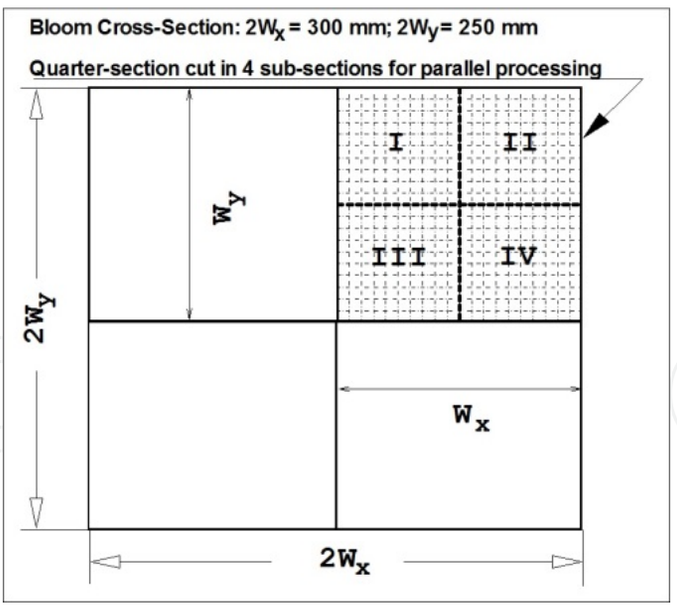

Figure 4. Illustration of the selected bloom quarter-section for the numerical solution of the 2D heat transfer equation. In roman numerals are depicted the four selected sub-sections upon which each CPU solved the temperature distribution using the Gauss-Seidel algorithm.

In this way, the computed results were stored in the disk and the system proceeded for the next time step; step-by-step the solidification front reached the center of the bloom. In average,

about 30–40 iterations per time step sufficed for convergence. The local cooling rates were computed at every nodal point, as follows:

$$C_R = \left(T\big|_{t+\Delta t} - T\big|_t \right) / \Delta t \tag{18}$$

7. Results and discussion

The Stomana bloom caster has a casting radius of 12 m, with M-EMS and no extra EMS or soft reduction along its four strands. Nevertheless, it is interesting to know the effect of critical casting parameters in order to maximize casting speed and hence, productivity, keeping the most attainable good internal porosity as much as possible. Consequently, the effect of parameters like U_c, SPH, ℓpkg, and a_g upon L_{SOL} was decided to be analyzed. Preliminary results showed that there were specific ranges of casting speeds U_c depending upon the selected steel grade; moving from MC to HC grades U_c should decrease, otherwise the required casting length for complete solidification L_{SOL} exceeded a lot the design value of the Stomana bloom caster that is close to 34 m. Figures 5 and 6 present typical computational results for the medium and high carbon steel grades selected at specific casting conditions. L_{SOL} values may vary a lot depending upon casting conditions and steel grades. For this reason, a reduced semi-factorial [33] computational experimental design was carried out in order to minimize the steps required to study the phenomenon.

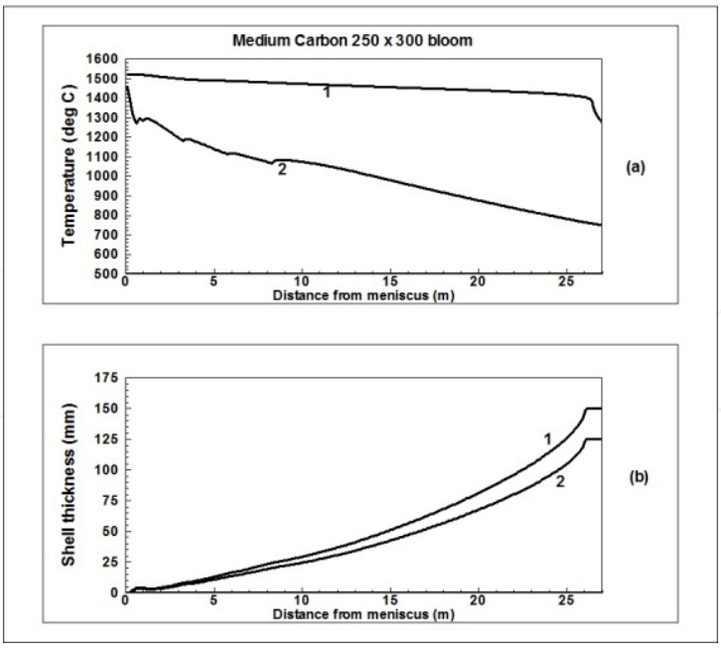

Figure 5. Casting results for the selected MC grade, for U_c = 0.55 m/min, SPH = 30 K, ℓpkg = 0.200, a_g = 12%. (a) Curves 1 and 2 show the centerline and surface temperatures, respectively. (b) Curves 1 and 2 show the shell thicknesses as they progress through the width (x-axis or horizontal direction) and the thickness (y-axis or vertical direction). The solidification or actual metallurgical length computed was 26.12 m. (Run no. 4, Table 2).

http://dx.doi.org/10.5772/60706

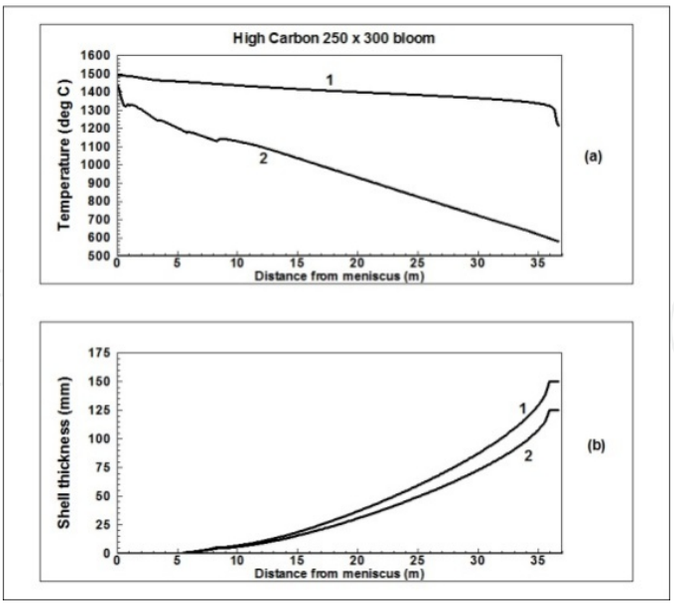

Figure 6. Casting results for the selected HC grade, for U_c = 0.55 m/min, *SPH* = 30 K, ℓpkg = 0.200, a_g = 12%. (a) Curves 1 and 2 show the centerline and surface temperatures, respectively. (b) Curves 1 and 2 show the shell thicknesses as they progress through the width (x-axis or horizontal direction) and the thickness (y-axis or vertical direction). The solidification or actual metallurgical length computed was 35.93 m. (Run no. 3, Table 2).

The adopted values for the casting parameters and the results for the required solidification lengths, for the MC and HC grades selected, are presented in Table 2. Initially it was designed for 12 cases; some more runs were added as of existing preliminary data (included in the statistical analysis).

The effect of air-gap formation upon the temperature distribution in the bloom corners was also verified in this study in accordance with a recent research work published in [7]. Specifically, Figure 7 depicts typical results revealing this important effect. Increasing the percentage of contact loss in the bloom corners due to air-gap formation inside the mold the exit-mold temperatures in the corners increase as well. On the other hand, a statistical analysis that was performed for the effect of the casting conditions upon the required solidification length for the two selected grades as presented in Table 2 showed that the air-gap formation inside the mold has no effect upon L_{SOL}. Probably this may be attributed to the fact that there is a lot of time for temperature re-distribution (soaking) due to conduction during the secondary cooling period, which is long enough as of the low casting speeds applied. Analysis of variance (ANOVA) was carried out using the R statistical package and the overall results are summarized in Table 3. Two things may be pointed out from the results presented in Table 3. First, similar behavior for the effects of the most critical factors upon the solidification length were found; in fact, an increase of 0.05 m/min upon casting speed seems to increase L_{SOL} by 2.4 m for MC, and by 3.2 m for HC, respectively. Similarly, an increase of 10°C upon superheat seems to increase L_{SOL} by 0.72 m for MC, and by 0.52 m for HC, respectively. The specific secondary water-cooling consumption has a negative effect for both grades, but unfortunately it cannot be increased appreciably due to potential surface defects on the blooms. Furthermore, the very good correlations deduced are attributed to the nature of the reduced semi-factorial design of runs that gave the maximum possible information to the ANOVA under the minimum number of tests.

	MC grade					HC grade				
Run no.	L_{SOL} *(m)*	U_c *(m/min)*	*SPH* (K)	ℓpkg *(liter/kg)*	a_g *(%)*	L_{SOL} *(m)*	U_c *(m/min)*	*SPH* (K)	ℓpkg *(liter/kg)*	a_g *(%)*
1	33.37	0.70	45	0.536	12	36.21	0.55	45	0.480	12
2	32.43	0.70	30	0.466	12	35.29	0.55	30	0.480	12
3	33.13	0.70	30	0.200	12	35.93	0.55	30	0.200	12
4	26.12	0.55	30	0.200	12	26.40	0.40	30	0.200	12
5	26.03	0.55	30	0.200	0	26.40	0.40	30	0.200	0
6	33.37	0.70	45	0.536	0	36.02	0.55	45	0.561	0
7	26.12	0.55	45	0.561	0	26.27	0.40	45	0.606	0
8	27.04	0.55	45	0.200	0	26.53	0.40	45	0.450	0
9	33.37	0.70	45	0.536	6	27.13	0.40	45	0.200	0
10	28.85	0.625	30	0.469	6	36.12	0.55	45	0.480	6
11	27.04	0.55	45	0.200	6	28.95	0.45	30	0.479	6
12	29.58	0.625	30	0.200	6	27.13	0.40	45	0.200	6
13	30.01	0.65	30	0.468	0	29.63	0.45	30	0.200	6
14	32.43	0.70	30	0.466	0	—	—	—	—	—

Table 2. Computational results for the effect of casting speed (U_c), superheat (*SPH*), specific secondary cooling-water consumption (ℓpkg), and air-gap percentage at the bloom corners (a_g) upon the required caster length for complete solidification (L_{SOL}), for the two selected steel grades

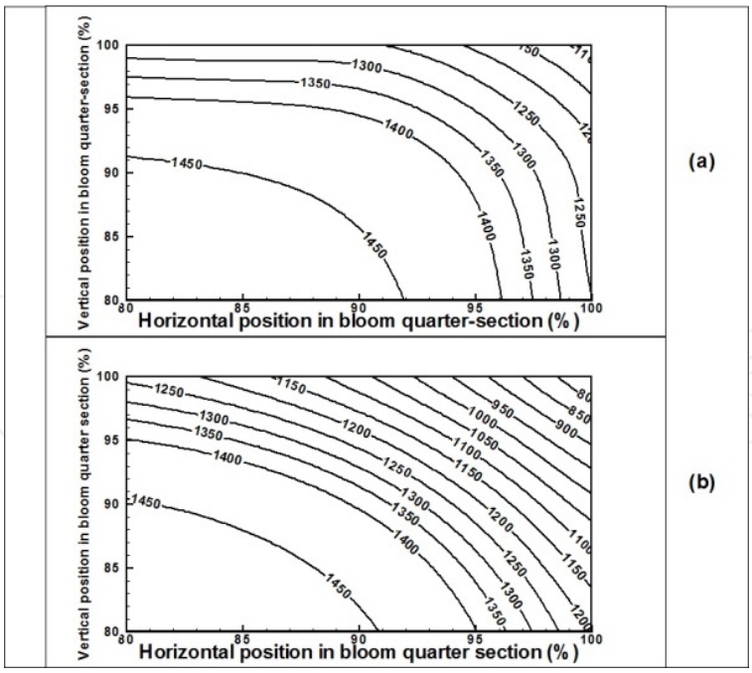

Figure 7. The effect of contact loss between the solidified shell and the mold upon the temperature distribution in the bloom corners, due to air-gap formation in these areas. The presented temperature distributions in the corner regions are from results obtained for MC steel cast at the following conditions: U_c = 0.55 m/min, *SPH* = 30 K, ℓpkg = 0.200, case (a) a_g = 12% (Run no. 4, Table 2), case (b) a_g = 0% (Run no. 5, Table 2).

http://dx.doi.org/10.5772/60706

	MC		HC	
Factor	**Regression coefficient**	**Statistical Significance**	**Regression coefficient**	**Statistical Significance**
U_c	47.589	***	64.064	***
SPH	0.0716	***	0.052	***
ℓpkg	–2.636	***	–2.209	***
Intercept	–1.782	***	–0.383	***
Correlation coefficient	0.9997		0.9999	
Standard error of estimate	0.049		0.0545	
F-value	16770, on 3 and 10 DF		26920, on 3 and 9 DF	

Table 3. Linear regression and ANOVA results for the factors affecting the solidification length as performed using R

In this way, a regression formula of the form

$$L_{sol} = b_0 + b_1 * U_C + b_2 * SPH + b_3 * \ell pkg \tag{19}$$

is derived, where *b*'s are the regression coefficients (Table 3) for MC and HC, respectively.

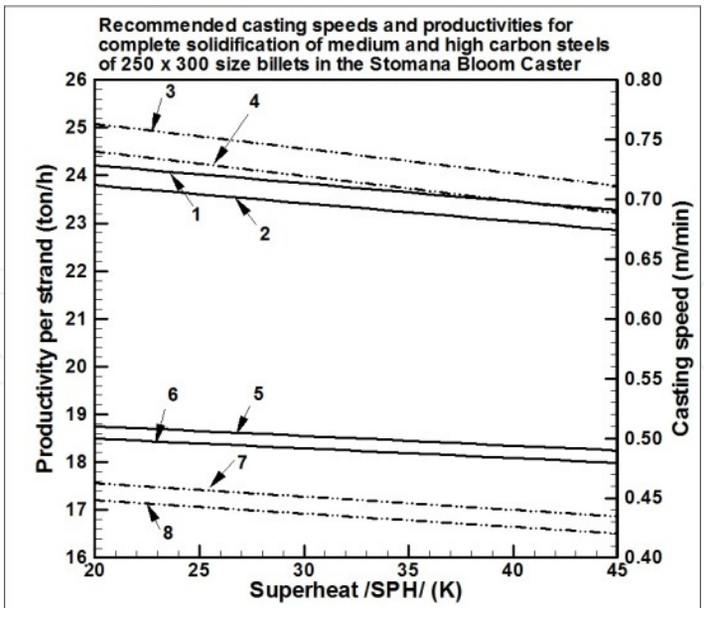

Figure 8. Casting speeds and productivities per strand in order to have complete solidification along the centerline at the point of cut-to-length products, for the selected MC and HC steels, and at various superheats. MC steel: Curves 1 and 3 represent the casting speed, and productivity for ℓpkg = 0.5, and 2 and 4 similar curves for ℓpkg = 0.2. HC steel: Curves 5 and 7 represent the casting speed and productivity for ℓpkg = 0.5, and 6 and 8 similar curves for ℓpkg = 0.2.

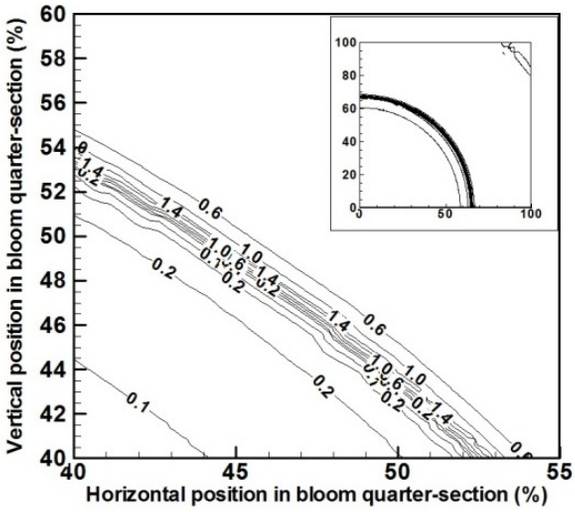

Figure 9. Typical local cooling-rate results as computed for the selected MC steel cast at the following conditions: U_c = 0.70 m/min, *SPH* = 30 K, ℓpkg = 0.200, a_g = 12% (Run no. 3, Table 2). The results presented correspond to the time instance of 1710 sec, or equivalently, to a position of 19.95 m from the meniscus-level.

More than 99% statistical importance is signified by 3-stars (***) on Table 3, according to R. Figure 8 summarizes the results presented on Table 3 in graphical form. For practical purposes the maximum allowable caster length was considered to be 33 m (instead of 34 m that the Stomana caster actually is), introducing a small safety factor.

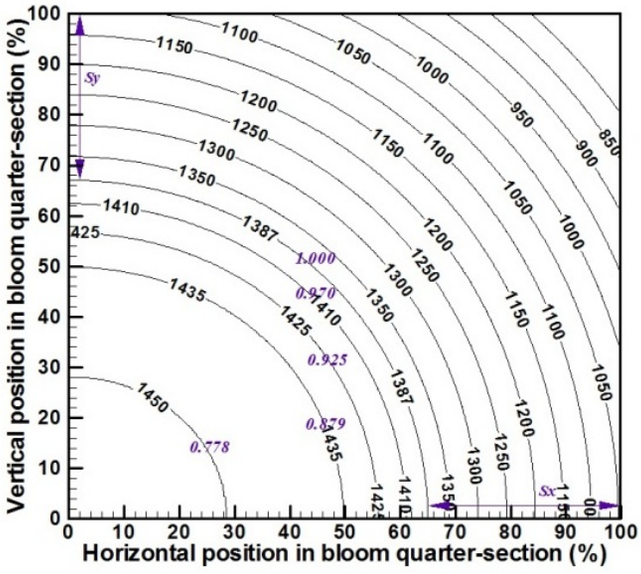

Figure 10. Temperature distribution inside a bloom section as computed for the selected MC steel cast at the following conditions: U_c = 0.70 m/min, *SPH* = 30 K, ℓpkg = 0.200, a_g = 12% (Run no. 3, Table 2). The results presented correspond to the time instance of 1710 sec, or equivalently, to a position of 19.95 m from the meniscus-level. Some solid fraction values are also presented (in purple color).

http://dx.doi.org/10.5772/60706

Figures 9 and 10 illustrate results for the local-cooling rates and temperatures inside a bloom for the MC grade selected, under the same casting conditions at a specific location from the liquid-steel meniscus level in the mold. Figure 9 shows that there is a distribution of local cooling-rate values at any instance inside the bloom. For this case, a simple statistical analysis gave an average value μ = 0.205 °C/s, a standard deviation σ = 0.140, and min and max values equal to 0 and 2.057, respectively. For this average value, the micro-segregation analysis gave a solidus temperature around 1389°C. This value is very close to the solidus temperature of 1387°C that the micro-segregation analysis gave for the computed cooling-rate conditions at the solidification front as depicted in Figure 10. The distances Sx and Sy show the corresponding shell thicknesses along the x and y axes. It is understood that the error would be tremendous if the shell thicknesses were computed based on the a priori solidus temperature (T_S*= 1435°C, Table 1) derived upon the chemical analysis only. Similar results are presented in Figures 11 and 12 for the HC grade selected.

Figure 11 depicts the local cooling rates inside a bloom section at about 24.98 m from the liquid steel meniscus level. In this case, the statistical analysis gave an average value for the local cooling rates of μ = 0.204 °C/s, with a standard cooling rate of 0.074, and min and max values of 0 and 1.682, respectively. The local micro-segregation analysis gave a solidus temperature of 1307°C which is shown in Figure 12, and which is very close to the solidus temperature of 1306°C computed from the average cooling-rate of a section at the instance under discussion. One may wonder about the large error upon the estimate of the shell thickness if the whole analysis relied only upon the a priori calculated value (T_S* = 1366°C) based on the HC selected chemical analysis – an error of about 60°C in absolute value, erroneously concluding almost 100% solidification at a very premature time!

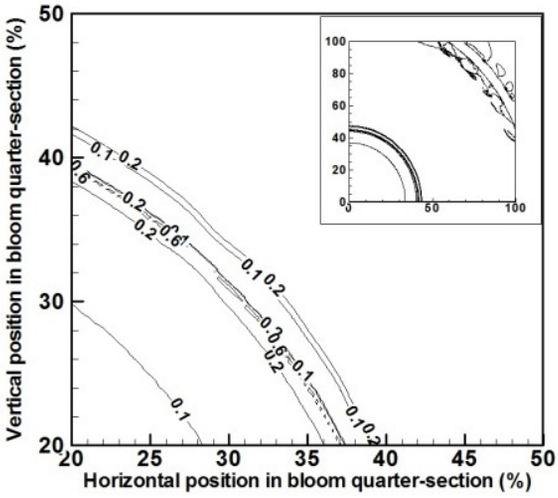

Figure 11. Typical local cooling-rates results as computed for the selected HC steel cast at the following conditions: U_c = 0.45 m/min, *SPH* = 30 K, ℓpkg = 0.200, a_g = 6% (Run no. 13, Table 2). The results presented correspond to the time instance of 3330 sec, or equivalently, to a position of 24.98 m from the meniscus-level.

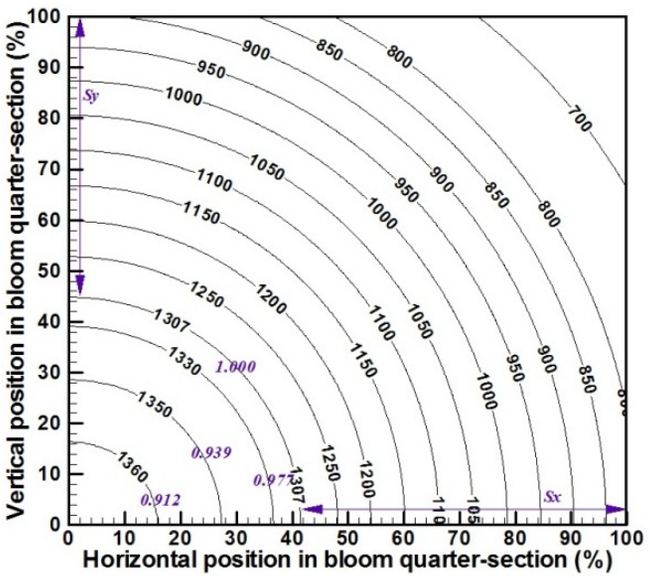

Figure 12. Temperature distribution inside a bloom section as computed for the selected HC steel cast at the following conditions: U_c = 0.45 m/min, *SPH* = 30 K, ℓpkg = 0.200, a_g = 6% (Run no. 13, Table 2). The results presented correspond to the time instance of 3330 sec, or equivalently, to a position of 24.98 m from the meniscus-level. Some solid fraction values are also presented (in purple color).

Some more results of this nature are presented in Figures 13 and 14 at different casting conditions than those presented in the previous set of data shown in Figures 9 and 10 for the MC steel grade selected. Figure 13 exhibits local cooling rates at an approximate distance of 25 m from the liquid steel meniscus level in the mold. In this case, a short statistical analysis for the local cooling rates gave an average value of μ = 0.264 °C/s, with a standard deviation of 0.087, and min and max values of 0.001 and 1.112, respectively.

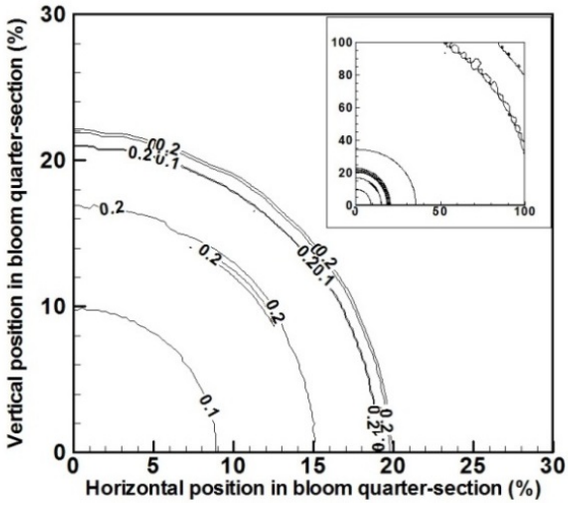

Figure 13. Typical local cooling-rate results as computed for the selected MC steel cast at the following conditions: U_c = 0.55 m/min, *SPH* = 45 K, ℓpkg = 0.561, a_g = 0% (Run no. 7, Table 2). The results presented correspond to the time instance of 2730 sec, or equivalently to an approximate position of 25.0 m from the meniscus-level.

http://dx.doi.org/10.5772/60706

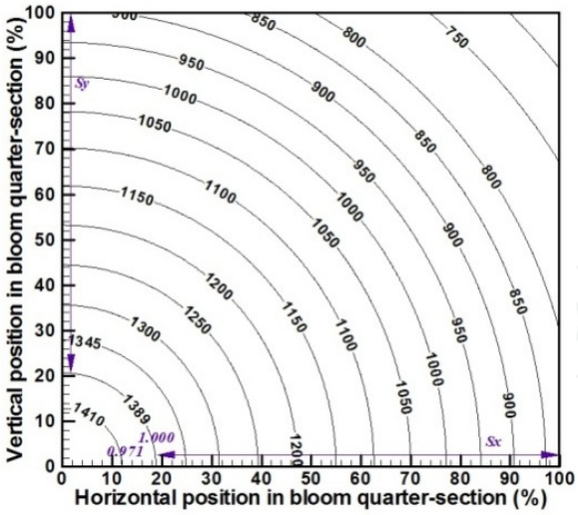

Figure 14. Temperature distribution inside a bloom section as computed for the selected MC steel cast at the following conditions: U_c = 0.55 m/min, *SPH* = 45 K, ℓpkg = 0.561, a_g = 0% (Run no. 7, Table 2). The results presented correspond to the time instance of 2730 sec, or equivalently to an approximate position of 25.0 m from the meniscus-level. Some solid fraction values are also presented (in purple color).

Figure 14 shows the temperature distribution inside the bloom section at the conditions presented in Figure 13. In this case, the computed solidus temperature at the solidification front was found to be 1389°C, a temperature that also defines the shell thicknesses (Sx and Sy) along the x and y axes.

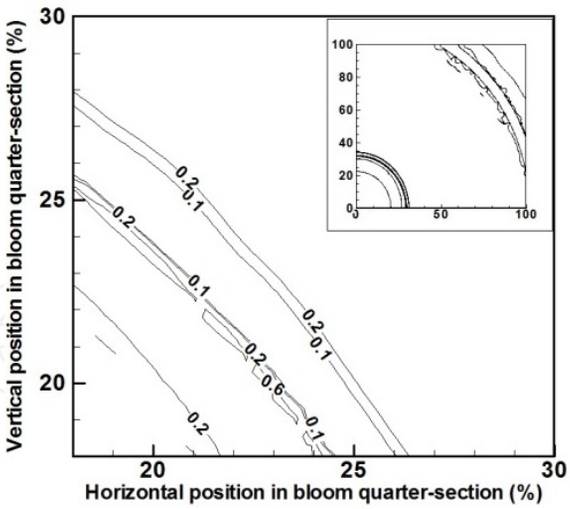

Figure 15. Typical local cooling-rate results as computed for the selected HC steel cast at the following conditions: U_c = 0.40 m/min, *SPH* = 45 K, ℓpkg = 0.200, a_g = 0% (Run no. 9, Table 2). The results presented correspond to the time instance of 3750 sec, or equivalently to a position of 25.0 m from the meniscus-level.

Similar results are also presented in Figures 15 and 16 for the HC steel grade selected. At different continuous casting conditions than the ones presented in Figures 11 and 12, these results show data just a couple of meters apart from the final stage of solidification. Figure

15 illustrates in graphical form that the local cooling rates remain as a distribution of values with an average value of μ = 0.230 °C/sec, with a standard error of σ = 0.073, and min and max values of 0 and 1.729, respectively. Figure 16 depicts the temperature distribution inside the bloom section, defining the shell thicknesses along the x and y axes (Sx and Sy), at the computed solidus temperature of 1306°C.

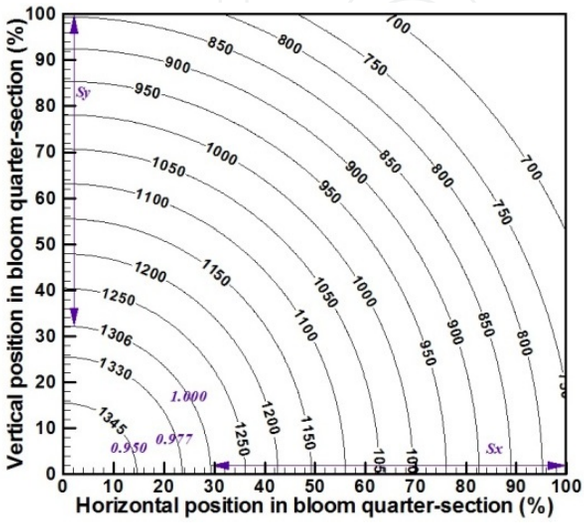

Figure 16. Temperature distribution inside a bloom section as computed for the selected HC steel cast at the following conditions: U_c = 0.40 m/min, *SPH* = 45 K, ℓpkg = 0.200, a_g = 0% (Run no. 9, Table 2). The results presented correspond to the time instance of 3750 sec, or equivalently to a position of 25.0 m from the meniscus-level. Some solid fraction values are also presented (in purple color).

One last comment about the computed values of local cooling rates: once the shell formation has been created inside the mold, the average values of the local cooling rates are more or less stabilized to specific values. For example, for the cases presented in the Figures 9 through 16, the overall average values for the local cooling rates are about 0.234°C/s for the MC and 0.217°C/s for the HC, respectively. Supplying these values to the micro-segregation model, the values of 1389°C and 1306°C for the solidus temperatures of the MC and HC grades can be deduced, respectively. In this way, a priori calculated values for the solidus temperatures may be used with better precision in heat transfer applications that rely upon preselected values only.

The prediction of the grain size of the solidified metal structure as described in Ref. [27], together with the percentage of the equiaxed zone that may be formed depending on the prevailing heat-transfer conditions may be one part for future work; another part could be the analysis of thermal stress-strain phenomena that act upon the solidifying shell.

8. Conclusions

The installation of strand EMS has been decided for the Stomana caster. The target is to come up with blooms having better internal soundness than the one presented in Figure 1. However, some fundamental points are covered with the help of this study. Summarizing:

http://dx.doi.org/10.5772/60706

- The casting conditions with respect to the required casting length for complete solidification have been analyzed, and the effect upon expected productivity per grade is known.
- The appreciation of the solidification phenomena is impossible without coupling the micro-segregation analysis, especially for medium and high carbon grades. Once the S-EMS is installed, the specific range of critical solid fractions required for the proper performance of the stirrers can be linked with the operating conditions of the caster.
- The difficulty in predicting the solidus temperature at varying cooling conditions especially for high carbon steels has been illustrated. Nevertheless, a shortcut that can generate solidus temperatures to be used as a priori values in heat transfer models has been presented; it only takes some runs for the appropriate heat-transfer models to compute average values for the local cooling rates, which then may be fed to standalone micro-segregation models to calculate the corresponding solidus temperatures. Consequently, simple heat transfer models can simulate casting with less error in the involved solidification phenomena for medium and high carbon steels, by taking as input the solidus temperatures derived in the aforementioned manner.
- The great importance of heat transfer analysis on the domain of medium and high carbon solidification is proven once more. It is of paramount importance that mankind has this kind of tool for shedding light into similar type of complex industrial conditions.

Nomenclature

a_g: Air gap factor. Percent of the bloom corner that lost contact to mold

C_p; Heat capacity in J kg K^{-1}

f_S; Solid fraction

h; Heat transfer coefficient, in W m^{-2} K^{-1}

k; Thermal conductivity, in W m^{-1} K^{-1}

L; Length, in m

L_{SOL}; Required caster length for complete solidification, in m

ℓpkg; Specific secondary cooling-water consumption, in liters of water/kg of steel

q; Heat flux, in W m^{-2}

S, S_c; Source term, constant term of S, in W m^{-3}

S_p; Source term that compensates for the temperature dependence of S, in W m^{-3} K^{-1}

SPH; Superheat, casting temperature – liquidus temperature, in °C or K

t, Δt; Time, time interval, in sec

T; Temperature in a position inside the bloom, or at a nodal point, in °C

T_L, T_S; Liquidus, solidus temperature, in °C

U_c; Casting speed, in m/min

W_x; Half-width of the bloom, along the (horizontal) x-axis, in m

W_y; Half-thickness of the bloom, along the (vertical) y-axis, in m

x, y, z; Spatial coordinates, in m

Δx, Δy; Distance between adjacent nodal points along the x- and y-axis, respectively, in m

ε; Emissivity

ϱ; Density, in kg m^{-3}

σ; The Stefan–Boltzmann constant, which is equal to 5.67 10^{-8} W m^{-2} K^{-4}

ω; Over-relaxation factor

Subscripts

0; Referring to an initial value

F, f; Fluid (WF referring to water as cooling fluid)

S, s; Surface, or solid

r, c; Radiation, convection

m; Average value, or referring to the mold

ag; Air gap is considered

Acknowledgements

The author is grateful to the top-management of Sidenor SA for the continuous support upon these types of studies, as well as for the permission of publishing this piece of work. My continuous gratitude and respect to Professor Rabi Baliga from the Mechanical Engineering Department of McGill University, Montreal, Canada, who introduced me to the field of computational fluid-flow and heat transfer should also be acknowledged.

Author details

Panagiotis Sismanis

Address all correspondence to: psismanis@sidenor.vionet.gr

Sidenor SA, Greece

References

[1] Henderson S., Scholes A., Clarke B.D. Continuous Casting of High-Carbon steels in Billet and Bloom Sections at Sub-Liquidus Temperatures. Technical Steel Research, Final Report, EUR 13623 EN, Belgium, 1991.

[2] Oh K.S., Chang Y.W. Macrosegregation Behavior in Continuously Cast High Carbon Steel Blooms and Billets at the Final Stage of Solidification in Combination Stirring. ISIJ Intl, Vol. 35, No. 7, 1995, pp. 866-875.

[3] Chowaniek F. Quality Improvement of Continuously Cast Round Billets. METALURGIJA, Vol. 47, No. 3, 2008, pp. 191-193.

[4] Luo S., Zhu M., Louhenkilpi S. Numerical Simulation of Solidification Structure of High Carbon Steel in Continuous Casting using Cellular Automaton Method. ISIJ Intl, Vol. 52, No. 5, 2012, pp. 823-830.

[5] Cibulka J., Bocek D., Huczala T., Cupek J. Possibilities of S-EMS utilization for the Improvement of Central Segregation in Continuously Cast Billets in Conditions of TŽ. Journal of Achievements in Materials and Manufacturing Engineering, Vol. 55, No. 2, December 2012.

[6] Rezende J., Schankies C., Alves C., Huettenmeister D., Senk D. Phase-Field Investigation of the Influence of the Solid-Liquid Interface Energy, Chemical Composition and Forced Convection on the Dendrite Growth Morphology for High Manganese Steels. In: 8th European Continuous Casting Conference and Symposium in Numerical & Physical Modeling, ASMET, 23-26 June 2014, Graz, Austria, pp. 124-132.

[7] Wang Y., Yang Z., Zhang X., Wang B., Liu Q. 3D Numerical Simulation of Flow and Solidification of Molten Steel in Bloom Continuous Casting Mold with Electromagnetic Stirring. In: 8th European Continuous Casting Conference and Symposium in Numerical & Physical Modeling, ASMET, 23-26 June 2014, Graz, Austria, pp. 144-158.

[8] Vazquez M., Poltarak G., Ferro S., Campos A., Cicutti C. Application of Mathematical Models to Optimize Operating Conditions during the Continuous Casting of Round Bars. In: 8th European Continuous Casting Conference and Symposium in Numerical & Physical Modeling, ASMET, 23-26 June 2014, Graz, Austria, pp. 179-188.

[9] Sgro A., Rinaldi M., Kunstreich S., Yves D. Recent Danieli Experiences for Electromagnetic Stirrer Optimization in Round Blooms Continuous Casting. In: 8th European Continuous Casting Conference and Symposium in Numerical & Physical Modeling, ASMET, 23-26 June 2014, Graz, Austria, pp. 1454-1461.

[10] Sgro A., Rinaldi M., Accardo G. A New Benchmark in Special Steel Casting: New Twin-Strand Vertical Caster at POSCO Specialty Steel, Korea. In: 8th European Con-

tinuous Casting Conference and Symposium in Numerical & Physical Modeling, ASMET, 23-26 June 2014, Graz, Austria, pp. 338-346.

[11] Tacke K-H. Irregular and Fluctuating Phenomena in Continuous Casting. In: 8th European Continuous Casting Conference and Symposium in Numerical & Physical Modeling, ASMET, 23-26 June 2014, Graz, Austria, pp. 699-708.

[12] Alvarez de Toledo G., Komenda J., Stewart B., Brune T., Frisk K. Influence of Composition and Continuous Casting Parameters on the Cracking of B-Micro-alloyed High Mn Steel Grades. In: 8th European Continuous Casting Conference and Symposium in Numerical & Physical Modeling, ASMET, 23-26 June 2014, Graz, Austria, pp. 709-718.

[13] Brune T., Haberl F., Senk D. Hot-Ductility and Precipitation Behavior of Boron in Nb-V-Ti Micro-alloyed Steels for CC. In: 8th European Continuous Casting Conference and Symposium in Numerical & Physical Modeling, ASMET, 23-26 June 2014, Graz, Austria, pp. 719-728.

[14] Rauter W., Reiter J., Srienc K., Brandl W., Erker M., Huemer K., Mair A. Soft Reduction at a Round Bloom Caster: Implementation and Results. In: 8th European Continuous Casting Conference and Symposium in Numerical & Physical Modeling, ASMET, 23-26 June 2014, Graz, Austria, pp. 811-820.

[15] Angelini L., Guerra F., Persi C., Straffelini G., Botelho P. Quality Improvement of the Acciaierrie di Calvisano CCM through the EM Multi-Stirring Technology: Preliminary Results. In: 8th European Continuous Casting Conference and Symposium in Numerical & Physical Modeling, ASMET, 23-26 June 2014, Graz, Austria, pp. 821-830.

[16] Chen M-H., Lu C-Y., Lin K-J., Kao C-L., Huang S-Y., Tsai M-F., Kuo A-N. Central Segregation Improvement of High Carbon Steels at CSC #3 Bloom Caster. In: 8th European Continuous Casting Conference and Symposium in Numerical & Physical Modeling, ASMET, 23-26 June 2014, Graz, Austria, pp. 831-838.

[17] Krajewski P., Krobath R., Bernhard C., Miettinen J., Louhenkilpi S., Ilie S., Schaden T. A Novel Approach for the Simulation of Surface Cracks Formation in Continuous Casting. In: 8th European Continuous Casting Conference and Symposium in Numerical & Physical Modeling, ASMET, 23-26 June 2014, Graz, Austria, pp. 1160-1169.

[18] Hahn S., Schaden T. DynaPhase: Online Calculation of Thermodynamic Properties during Continuous Casting. In: 8th European Continuous Casting Conference and Symposium in Numerical & Physical Modeling, ASMET, 23-26 June 2014, Graz, Austria, pp. 1170-1180.

[19] Thomas B.G., Samarasekera I.V., Brimacombe J.K. Mathematical Modeling of the Thermal Processing of Steel Ingots: Part I. Heat Flow Model. Metallurgical Transactions B, Vol. 18B, 1987, pp. 119-130.

[20] Won Y-M., Thomas B.G. Simple Model of Micro-segregation During Solidification of Steels. Metallurgical Transactions A, Vol. 32A, 2001, pp. 1755-1767.

[21] Carslaw H.S., Jaeger J.C. Conduction of Heat in Solids. Oxford University Press, New York, 1986.

[22] Incropera F.P., DeWitt D.P. Fundamentals of Heat Transfer. John Wiley & Sons, New York, 1981.

[23] Patankar S.V. Numerical Heat Transfer and Fluid Flow. Hemisphere Publishing Corporation, Washington, 1980.

[24] Yoon U-S., Bang I-W., Rhee J-H., Kim S-Y., Lee J-D., Oh K-H. Analysis of Mold Level Hunching by Unsteady Bulging during Thin Slab Casting. ISIJ International, Vol. 42, No.10, 2002, pp. 1103-1111.

[25] Churchill S.W., Chu H.H.S. Correlating Equations for Laminar and Turbulent Free Convection from a Horizontal Cylinder. Int. J. Heat Mass Transfer, Vol.18, 1975, pp. 1049-1053.

[26] Burmeister L.C. Convective Heat Transfer. John Wiley & Sons, 1983, p. 551.

[27] Cabrera-Marrero J.M., Carreno-Galindo V., Morales R.D., Chavez-Alcala F. Macro-Micro Modeling of the Dendritic Microstructure of Steel Billets by Continuous Casting. ISIJ International, Vol. 38, No. 8, 1998, pp. 812-821.

[28] Sismanis P. Heat Transfer Analysis of Special Reinforced NSC-Columns under Severe Fire Conditions. International Journal of Materials Research, Vol. 101, March 2010, DOI 10.3139/146.110290, pp. 417-430.

[29] Sismanis P. Modeling Solidification Phenomena in the Continuous Casting of Carbon Steels. In: Amimul Ahsan (ed.). Two Phase Flow, Phase Change and Numerical Modeling. Rijeka: InTech; 2011. p.121-148. Available from by http://www.intechopen.com/books/two-phase-flow-phase-change-and-numerical-modeling/modeling-solidification-phenomena-in-the-continuous-casting-of-carbon-steels (accessed 21 August 2014).

[30] Sismanis P. The Effect of Local Cooling Rates upon Solidification Phenomena in the Continuous Casting of Carbon Steels. In: 8th European Continuous Casting Conference and Symposium in Numerical & Physical Modeling, ASMET, 23-26 June 2014, Graz, Austria, pp. 1462-1471.

[31] Anderson D.A., Tannehill J.C., Pletcher R.H. Computational Fluid Mechanics and Heat Transfer. Hemisphere Publishing Corporation. Washington. 1984.

[32] James M., Smith G.M., Wolford J.C. Applied Numerical Methods for Digital Computation with FORTRAN and CSMP. Harper & Row Publishers. New York. 1977.

[33] Montgomery D.C. Design and Analysis of Experiments. 2nd ed., John Wiley, New York, 1984.

IntechOpen